M A Lohe

Conformist-contrarian interactions and amplitude dependence in the Kuramoto model

Physica Scripta, 2014; 89(11):115202-1-115202-10

Conformist-contrarian interactions and amplitude dependence in the Kuramoto model

M A Lohe

Centre for Complex Systems and Structure of Matter, Department of Physics, The University of Adelaide, South Australia 5005, Australia

E-mail: Max.Lohe@adelaide.edu.au

Abstract. We derive exact formulas for the frequency of synchronized oscillations in Kuramoto models with conformist-contrarian interactions, and determine necessary conditions for synchronization to occur. Numerical computations show that for certain parameters repulsive nodes behave as conformists, and that in other cases attractive nodes can display frustration, being neither conformist nor contrarian. The signs of repulsive couplings can be placed equivalently outside the sum, as proposed in *Phys. Rev. Lett.* **106** (2011) 054102, or inside the sum as in *Phys. Rev.* E **85** (2012) 056210, but the two models have different characteristics for small magnitudes of the coupling constants. In the latter case we show that the distributed coupling constants can be viewed as oscillator amplitudes which are constant in time, with the property that oscillators of small amplitude couple only weakly to connected nodes. Such models provide a means of investigating the effect of amplitude variations on synchronization properties.

PACS numbers: 05.45.Xt, 89.75.-k

Submitted to: *Phys. Scr.*

1. Introduction

The Kuramoto model has been widely studied as a model of synchronized behavior in complex systems, with a variety of applications [1]. In the simplest form the coupling κ is constant over the network, yet more realistically one would expect to have distributed couplings which vary in magnitude with the node, or possibly with each link, of the network. A further generalization [2] is to allow a variable sign for the coupling, leading to a tension, or frustration, in the system according to whether the negative couplings restrict or even prevent synchronization occurring. Generally, nodes behave as contrarian or conformist, as defined in [2], according to the sign of the coupling, although we find here that other synchronized configurations can also occur. The role of contrarian nodes in suppressing synchronization is discussed in [3], and general properties of attractive and repulsive couplings are studied in [4, 5], sometimes for identical natural frequencies [6, 7]. Of particular interest is the possibility of a glass transition [8] (see the discussion in [2]), and we find here numerical examples for certain parameter sets in which some nodes display frustration, behaving as neither conformist nor contrarian. For applications of phase-repulsive models, see the introductory remarks in [9], including a discussion of activatory and repressory interactions in phase oscillator models.

The conformist-contrarian model proposed in [2] consists of a system of N oscillators with variables $\theta_i(t)$ defined by the N equations:

$$\dot{\theta}_i = \omega_i + \frac{\kappa_i}{N}\sum_{j=1}^{N}\sin(\theta_j - \theta_i), \tag{1}$$

where κ_i are nonzero coupling coefficients of variable sign that depend only on the node i, and ω_i is the natural frequency of the ith oscillator. Three kinds of long term behaviour are identified in [2]: incoherent states, π-states, and travelling wave states, depending on the various parameters and the initial values. The analysis in [2], which is restricted to the special case $N \to \infty$, has been extended in [10] to more general distributions of frequencies and couplings κ_i, see also [11, 12]. Phase lag effects combined with positive and negative coupling strengths have been investigated in [13], but only for $N \to \infty$.

Kuramoto models with variable (asymmetric) couplings κ_i are well-known, having been previously considered in the context of synchronization transitions [14], also in power networks (see for example [15] equations (2.3), and [16] equation (2.8)), but usually only for $\kappa_i > 0$. Variable couplings also appear in communities of phase oscillators, see for example [17] (with further references within) with both attractive and repulsive couplings, and in phase-repulsive networks of oscillators [9]. Other recent work examines the effect of a pinning force in a conformist-contrarian model [18] for a system with identical frequencies.

Our considerations apply for arbitrary but finite N and for any ω_i. We show that in the phase-locked synchronized system there is no distinction between π-states and travelling wave states, and we derive a formula for the synchronization frequency Ω

which, as noted in [2, 11], differs from the mean of the frequencies ω_i. This explicit formula provides information on allowable synchronized configurations, for example Ω can be much larger than any local frequency ω_i, and singular points of the formula indicate transitions to different configurations, as we discuss below. We investigate synchronization properties as a function of the scaling parameter κ, defined as the maximum norm of the N-vector κ_i, and observe that κ must exceed a critical value for synchronization to occur. Numerical results confirm some of the properties found in [2], such as the grouping of nodes under certain conditions as either conformist or contrarian, but we also find interesting exceptions such as frustrated configurations. We show that the separation of nodes into two groups with a phase lag of π, also discussed in [3], is an artifact of the coordinate definitions, and that the coupling sign can appear equivalently either outside or inside the sum over j in (1), as proposed in [19]. In some cases the two models discussed in [2, 19] are dynamically identical, but for very small couplings there are significant differences. We show that coupling constants inside the sum can be interpreted as oscillator amplitudes, thereby resolving a difficulty regarding the modelling of amplitude variations in the standard Kuramoto model, which is insensitive to distributed amplitudes.

2. Phase-locked synchronization

In phase-locked synchronization all nodes oscillate at a common frequency Ω, and so solutions to (1) take the form

$$\theta_i(t) = \Omega\, t + \theta_i^0, \tag{2}$$

where the angles θ_i^0 are constant in time. We investigate analytically the conditions under which these solutions exist, i.e. we study all solutions of (1) which take the form (2). Such solutions comprise the synchronization manifold ([1], Section 4.1). We investigate numerically the time-dependent properties of the system (1), such as stability, and determine numerically whether the system converges to a solution of the form (2). It is useful to define, as usual, the order parameter $r(t)$ according to

$$r(t) = \frac{1}{N}\left|\sum_{i=1}^{N} \mathrm{e}^{\mathrm{i}\theta_i(t)}\right|, \tag{3}$$

then $0 \leqslant r(t) \leqslant 1$. We are interested in the asymptotic value of $r(t)$, in particular whether $r(t)$ is constant for large t, which is characteristic of the phase-locked solutions (2). Hence, if this limit exists, we define $r_\infty = \lim_{t\to\infty} r(t)$ then for the solutions (2) r_∞ satisfies

$$r_\infty \mathrm{e}^{\mathrm{i}\psi} = \frac{1}{N}\sum_{i=1}^{N} \mathrm{e}^{\mathrm{i}\theta_i^0} \tag{4}$$

for some angle ψ, which may be regarded as the average of the angles θ_i^0. A constant asymptotic value for $r(t)$ does not by itself demonstrate that the system has synchronized, rather, we evaluate the average frequency $\Omega = \sum_i \dot{\theta}_i(t)/N$ numerically

at some time in the asymptotic region, and then verify that $\sum_i |\dot{\theta}_i - \Omega|$ is zero within numerical error. This demonstrates that each node is oscillating at the frequency Ω, i.e. that phase-locked synchronization has indeed occurred.

It is convenient to define the scaling variable κ by

$$\kappa = \max_i |\kappa_i|, \tag{5}$$

together with $\hat{\kappa}_i = \kappa_i/\kappa$, then $|\hat{\kappa}_i| \leqslant 1$ for all i, i.e. $\hat{\kappa}_i$ is an N-vector of unit length in the maximum norm. We regard $\hat{\kappa}_i$ as fixed and derive properties of r_∞ as a function of κ, where κ can be varied by rescaling the time variable t and the frequencies ω_i in (1). By substituting (2) into (1) we obtain the N algebraic equations

$$\Omega = \omega_i + \kappa_i\, r_\infty \sin(\psi - \theta_i^0). \tag{6}$$

Upon solving these equations for θ_i^0 and substituting into (4), we obtain the complex consistency equation

$$r_\infty = \frac{1}{N}\sum_{i=1}^{N} \exp\left[\mathrm{i}\sin^{-1}\left(\frac{\omega_i - \Omega}{\kappa_i\, r_\infty}\right)\right]. \tag{7}$$

The imaginary part, which reads $\sum_i(\omega_i - \Omega)/\kappa_i = 0$, leads to the explicit frequency formula

$$\Omega = \left(\sum\nolimits_i \frac{\omega_i}{\kappa_i}\right) \Big/ \left(\sum\nolimits_i \frac{1}{\kappa_i}\right). \tag{8}$$

Ω is invariant under rescaling of the couplings κ_i, and can become arbitrarily large if, for example, ω_i/κ_i is of order unity for every i and the denominator $\sum_i(1/\kappa_i)$ is arbitrarily small. By choice of reference frame, however, we can always set $\Omega = 0$, since (1) is invariant under $\theta_i \to \theta_i + \omega_0 t, \omega_i \to \omega_i + \omega_0$ for any constant ω_0, and so we may always choose $\Omega = 0$ by a suitable choice of ω_0. There is therefore no distinction between the π-states and the travelling wave states identified in [2], each of which are characterized by a constant value for r_∞, and for either of which we may choose $\Omega = 0$ in a suitable rotating reference frame.

The real part of (7) leads to an equation which implicitly determines $r_\infty(\kappa)$ as a function of κ:

$$r_\infty = \frac{1}{N}\sum_{i=1}^{N} s_i \sqrt{1 - \left(\frac{\omega_i'}{\kappa\, r_\infty}\right)^2}, \tag{9}$$

where the unknown signs $s_i = \pm 1$ appear in the evaluation of the function $\cos\sin^{-1}$, and

$$\omega_i' = \frac{\omega_i - \Omega}{\hat{\kappa}_i}, \tag{10}$$

which satisfies $\sum_i \omega_i' = 0$, with Ω given by (8), and $\kappa_i = \kappa\hat{\kappa}_i$. Equation (9) has previously been investigated in [20] (with positive signs only) and in [21]. If a solution r_∞ exists then $|\omega_i'| \leqslant \kappa r_\infty \leqslant \kappa$ for all i hence, for synchronization to occur, it is necessary that $\kappa \geqslant \max_i |\omega_i'|$. If $\hat{\kappa}_i$ is very small for some node i then $|\omega_i'|$ is very large and so κ must

be correspondingly large. Generally, κ must be larger than a critical value κ_c, as shown in [21], as also follows from our considerations in Section 5.2.

If the system synchronizes then (9) is satisfied for some combination of signs s_i which are determined by the stability of the phase-locked solution (2). We confirm this numerically, however it is not *a priori* evident as to which combination of signs the system will select. In those cases where the synchronized solution is only locally stable, we find that the signs depend on the initial values $\theta_i(0)$. For the standard Kuramoto model for which $\kappa_i = \kappa$ is positive and independent of i, we have $s_i = 1$ for all i, as is proved in [20]. Consistent with this we find numerically that for many, but not all, cases considered below $s_i = \operatorname{sgn} \kappa_i$, and so $s_i = 1$ whenever $\kappa_i > 0$.

Consider now the limit $\kappa \to \infty$ in (9), with ω_i' fixed, and let us assume that $\lim_{\kappa\to\infty} r_\infty(\kappa)$ is nonzero. (This is not always the case, see the discussion in Section 3.4). A solution to (9) then exists only if $\sum_i s_i \geqslant 0$, since $r_\infty \geqslant 0$. If $s_i = \operatorname{sgn} \kappa_i$, which is the case for the results in [2], then at least 50% of the couplings κ_i must be positive, although this is neither a necessary nor sufficient condition for synchronization to occur. In the example discussed in Section 3.4 we find synchronized configurations for $N = 19$ with 10 repulsive nodes and 9 attractive nodes. If we choose identical natural frequencies $\omega_i = \omega$, then $\Omega = \omega$, as follows from (8), and from (10) $\omega_i' = 0$, and hence

$$r_\infty = \frac{1}{N} \sum_{i=1}^{N} s_i. \tag{11}$$

3. Numerical investigations

Of the many solutions r_∞ to (9), arising from the various sign combinations, relatively few lead to stable configurations. We investigate the stability of any solutions numerically, showing that there exist two types of globally stable solutions (Sections 3.2,3.3) as well as other locally stable solutions (Sections 3.4, 5.3), some of which display frustration behaviour. Global stability implies that if the system synchronizes for any particular set of initial values $\theta_i(0)$, then it also synchronizes to the same final configuration for all other randomly generated initial values. Local stability implies that the system synchronizes to a given configuration for some but not all initial values; in some cases it may synchronize for all initial values, but to different equilibrium configurations.

3.1. Numerical methods

We solve the evolution equations (1) numerically over a wide range of values for N, from $N \leqslant 10$ up to $N = 1000$. For the examples in Sections 3.2–3.4 we choose small N in order to demonstrate various specific properties. We consider globally coupled networks (all-to-all coupling), except as described in Section 5.3.

The initial values $\theta_i(0)$ are selected at random from a uniform distribution in $[0, 2\pi]$. For nodes with negative couplings the unit coefficients $\hat{\kappa}_i$ are selected at random from a

uniform distribution in $[-1, 0)$, and for positive couplings from the interval $(0, 1]$, with an adjustable ratio of positive to negative couplings. We usually choose this ratio so that 50% or more of the couplings are positive, but with some exceptions, see the example discussed below in Section 3.4. The couplings are normalized so that $\max_i |\hat{\kappa}_i| = 1$. The natural frequencies ω_i appear in (9) only in the ratio $\omega_i/(\kappa\hat{\kappa}_i)$ and so by a choice of scale κ we may assume that $|\omega_i/\hat{\kappa}_i| \leqslant 1$ for every node i. Hence, for each i we select ω_i at random from a uniform distribution in the interval $[-|\hat{\kappa}_i|, |\hat{\kappa}_i|\,]$.

We choose a value for κ which is sufficiently large that the N inequalities (27) below are all satisfied, which does not, however, guarantee that the system will synchronize, and we then integrate (1) for $0 \leqslant t \leqslant t_{\text{final}}$. As a check on the accuracy of this solution we verify that the constant of the motion defined by (23) below is in fact constant to within a certain tolerance. Specifically, we define $F(t)$ to be the difference between the two sides of (23), then we evaluate $|F(t)|$ over a range of points t in the interval $[0, t_{\text{final}}]$ and find the maximum such value, which defines the tolerance, i.e. the accuracy of the solution. For 32-bit arithmetic this tolerance is usually of the order of 10^{-12}, but by increasing the precision settings in the integration routine we are able to achieve tolerances of 10^{-40}, sometimes much less. In particular, we have verified that the synchronized configurations shown in figures 1,2, and their associated properties, are accurate to within a tolerance of 10^{-40}.

Having found a numerical solution we evaluate $r(t)$ as defined by (3). Phase-locked synchronization occurs, following an initial transient, at a time $t = t_{\text{asymp}}$ when $r(t)$ attains a constant asymptotic value. Failure to achieve a constant value can indicate that: (a) a larger value of κ is required, i.e. the chosen value for κ is less than the critical value κ_c; (b) the number of positive couplings is not large enough to allow the system to synchronize; (c) the system is only locally stable for the selected parameters ω_i, κ_i, and might synchronize for some, but not all, sets of initial values $\theta_i(0)$. In order to determine the accuracy of the synchronization we evaluate the maximum value of $|r(t) - r(t_{\text{final}})|$ over a range of points t in the interval $[t_{\text{asymp}}, t_{\text{final}}]$; if this is not sufficiently small (i.e. close to or less than the tolerance achieved as described above), we increase both t_{asymp} and t_{final}, sometimes by several orders of magnitude, until $|r(t) - r(t_{\text{final}})|$ is less than the preset tolerance for all t in $[t_{\text{asymp}}, t_{\text{final}}]$.

The common frequency of oscillation is determined at or near $t = t_{\text{final}}$ as the average $\Omega = \sum_i \dot{\theta}_i/N$. We then verify that $\sum_i |\dot{\theta}_i - \Omega|$ is numerically zero, i.e. is less than the preset tolerance, which confirms that all nodes are indeed oscillating at the common frequency Ω, and that all trajectories $\theta_i(t)$ are numerically indistinguishable from the solutions (2) of the synchronization manifold. In all cases where synchronization occurs we find that this computed value of Ω agrees numerically with the formula (8). We also verify that (9) is satisfied for some combination of signs s_i. As already mentioned, synchronization occurs only if the percentage of positive couplings is sufficiently large, and only if κ is larger than a critical value which depends on the coefficients $\hat{\kappa}_i$ and the frequencies ω_i. Evidently, there must be enough attractive nodes, and of sufficient strength, to overcome the repulsive nodes.

The synchronized configurations are generally of two types, depending on the sign of the denominator in (8), but we have also detected exceptional cases, discussed in Section 3.4 below and later also in Section 5.3. Define the average unit coupling $\kappa_{\rm av}$ by

$$\frac{1}{\kappa_{\rm av}} = \frac{1}{N}\sum_{i=1}^{N}\frac{1}{\hat{\kappa}_i}, \tag{12}$$

as appears in the denominator of (8). The configurations for which $\kappa_{\rm av} > 0$ are discussed in Section 3.2, and those for which $\kappa_{\rm av} < 0$ are discussed in Section 3.3, and are in both cases globally stable, whereas the configurations in Section 3.4 are only locally stable.

In our simulations the parameters ω_i, κ_i are selected at random, so that zero values of either the denominator or numerator in (8) do not occur, which also means that we do not detect any special synchronized configurations that can occur only for particular combinations of parameters.

3.2. Positive average coupling

If $\kappa_{\rm av} > 0$ and the system has synchronized, then (9) is satisfied with the signs given by $s_i = \operatorname{sgn}\kappa_i$. This is consistent with the results in [2], except that we do not distinguish between π-states and travelling waves, as previously explained. The repulsive and attractive nodes each group together with contrarian/conformist behaviour, respectively, as described in [2]. The example in figure 1(a) for $N = 50, \kappa = 30$, with $\kappa_{\rm av} > 0$, shows the synchronized nodes plotted on a common unit circle, with the 27 attractive nodes marked in blue, and the remaining 23 repulsive nodes in red. The separation into conformist and contrarian groups according to the sign of κ_i is evident. The computed frequency Ω agrees with the formula (8) to within the tolerance 10^{-40}, and similarly equation (9) is satisfied to the same tolerance. The synchronized configuration is globally stable, and so the final state of the system is independent of the initial values.

We evaluate the phase difference between the two groups (red and blue) shown in figure 1(a) by defining the average phase ψ of each group according to the formula (4), except that the sum extends only over either the repulsive or attractive nodes. We find that the difference between these two averages is approximately, but not exactly, π, corresponding to the fact that the two groups are diametrically opposed. This corresponds well with Figure 1(c) of [2].

It is instructive to consider the special case in which the frequencies ω_i are identical, $\omega_i = \omega$ for all i, but where the parameters $\hat{\kappa}_i$ are generated at random as described above. Then from (8), $\Omega = \omega$ and $\omega_i' = 0$, where ω_i' is defined in (10), and r_∞ is given by (11). If there are p positive nodes, $N-p$ negative nodes, and $\kappa_{\rm av} > 0$, then for the configurations considered in this section (with $s_i = \operatorname{sgn}\kappa_i$) we always have $r_\infty = (2p-N)/N$, as may be verified numerically. The conformist and contrarian groups are co-located, respectively, i.e. the offset angles θ_i^0 given by (2) are all equal within each group. The phase difference in such cases is π, within numerical tolerance, regardless of whether ω is zero or nonzero.

3.3. Negative average coupling

The case $\kappa_{\rm av} < 0$ occurs when there are one or more small negative coefficients $\hat{\kappa}_i$. Then, provided the system has synchronized, we find that (9) is satisfied with the signs given by $s_i = \operatorname{sgn} \kappa_i$ for all i, except for one particular negative (repulsive) node for which $s_i = 1$. This node corresponds to the repulsive node i of maximum value, that for which $1/|\kappa_i|$ takes its maximum value. We consider here the case where there is precisely one such node. Because of the sign change, this particular repulsive node behaves as a conformist. In figure 1(b), for which the parameters $\omega_i, \hat{\kappa}_i$ are unchanged from those of figure 1(a) except for the value of $\hat{\kappa}_i$ at the repulsive node of maximum value, we have $\kappa_{\rm av} < 0$, and the plot shows that this repulsive node (red) is now grouped with the positive nodes (in blue). Again, the synchronized configuration is globally stable.

For the case of identical frequencies $\omega_i = \omega$ we have $\Omega = \omega$ as before. If there are p attractive nodes and if $\kappa_{\rm av} < 0$, there are $p + 1$ positive signs s_i, and so now according to (11), $r_\infty = (2p + 2 - N)/N$. Again, all nodes are co-located within each group, with a phase difference of π.

For both examples (a,b) synchronization occurs also for all values of κ larger than the plotted value ($\kappa = 30$), with the respective groupings being maintained, except that the grouping becomes tighter as κ increases; also the phase difference between the two groups approaches π as κ increases. We have also performed simulations for larger values of N up to $N = 1000$, for randomly generated parameters κ_i, ω_i, and find behaviour similar to that shown in figures 1(a,b). Synchronized configurations correspond to one of these figures depending on the sign of $\kappa_{\rm av}$, and both the frequency formula (8) and equation (9) are in all cases satisfied to within tolerance.

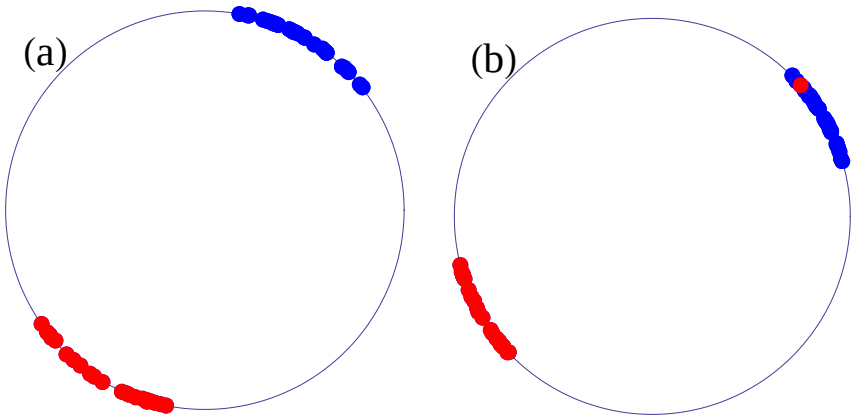

Figure 1. Separation of nodes for (a) $\kappa_{\rm av} > 0$ into conformist (blue) and contrarian (red) groups, and (b) for the case $\kappa_{\rm av} < 0$, showing one repulsive node (in red) grouped with the conformist nodes (in blue).

3.4. Locally stable configurations

There also exist synchronized configurations which unlike those in the previous Sections 3.2,3.3 are only locally stable. In such cases we find that the signs s_i differ from $\operatorname{sgn}\kappa_i$ at one or more nodes depending on the initial values $\theta_i(0)$, as is indicated by the value of r_∞ which takes different values depending on $\theta_i(0)$. Stability for such cases is therefore only local, and depends on a delicate balance of strength between competing attractive and repulsive nodes.

Frustrated synchronization occurs when one or more nodes is neither conformist nor contrarian. Two examples of frustration, for $N = 19, \kappa = 1000$, with 10 repulsive nodes and 9 attractive nodes, are shown in figures 2 (a,b), where the parameters κ_i, ω_i are the same for each figure, only the initial values are different. In each case there is one particular node, the one corresponding to the minimum positive value of κ_i, which does not group with either the conformist or contrarian nodes. There is also one repulsive node which groups with the conformist nodes, even though $\kappa_{\rm av} > 0$, as is evident in both figures. For this particular example there are also other locally stable configurations not shown, but always with the same frustrated node. The system synchronizes to one of these locally stable configurations for any set of initial values.

This frustration behaviour is maintained as κ increases to arbitrarily large values. This occurs because $r_\infty(\kappa)$, regarded as a function of κ, becomes arbitrarily small as κ increases, and we find numerically that $\kappa\, r_\infty(\kappa)$ is constant for large κ. By contrast, for the configurations of the previous Sections 3.2,3.3, r_∞ is nonzero for large κ.

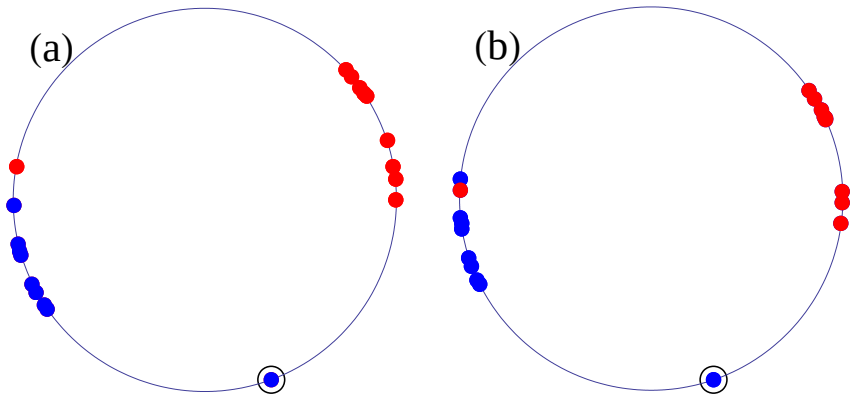

Figure 2. An example for $N = 19$ of two synchronized configurations for identical parameters but different initial values showing frustration, in which one node (circled) is neither conformist nor contrarian, even for large κ.

There are also locally stable configurations to which the system synchronizes for some initial values, but does not synchronize at all for other values. This can occur when the frequencies ω_i are identical, for example $\omega_i = 0$ at all nodes, with couplings κ_i for which $\kappa_{\rm av} < 0$. We have found an example with three such repulsive nodes, each with an identical value for κ_i that is also the largest negative value, where synchronization occurs in which two repulsive nodes, not just one as described in Section 3.3, group together

with the conformist nodes. Because the frequencies are identical all nodes group into two separate co-located groups with a phase difference of π; one group consists only of repulsive nodes, the other consists of all the attractive nodes plus the two repulsive nodes. We do not consider these configurations further, as our investigations are restricted primarily to generic parameter sets, which take random values. We mention other locally stable configurations in Section 5.3.

4. Phase lag equivalence

It is observed in [2] for the configurations analyzed there that contrarian nodes differ in their collective phase from conformist nodes by approximately π, see Figure 1 in [2]. This is evident also in figure 1(a) above, and we have also defined and calculated the precise phase difference as described in Section 3.2. Since the signs that appear in (9) are given in this case by $s_i = \operatorname{sgn}\kappa_i$, the separated nodes correspond precisely to the positive and negative signs of κ_i. The equivalence of this model and the phase lag model of Sakaguchi and Kuramoto [22] has been noted in [2], also [3]. We can make this equivalence precise by writing the interaction terms of (1) in the form $|\kappa_i| \sum_j \sin(\theta_j - \theta_i - \alpha_i)/N$, where the phase lag α_i is given

$$\alpha_i = \frac{\pi}{2}\left(1 - \operatorname{sgn}\kappa_i\right), \tag{13}$$

and is equal to zero ($\kappa_i > 0$), or π ($\kappa_i < 0$). We consider therefore the following Sakaguchi-Kuramoto model with distributed phase lag α_i defined by

$$\dot{\theta}_i = \omega_i + \frac{\kappa_i}{N}\sum_{j=1}^{N}\sin(\theta_j - \theta_i - \alpha_i). \tag{14}$$

The model (1) is equivalent to the (14) with κ_i replaced by $|\kappa_i|$, with a phase lag of either $\alpha_i = 0$ or $\alpha_i = \pi$ at the ith node. Define

$$\varphi_i = \theta_i - \alpha_i, \tag{15}$$

then with respect to these φ_i variables the synchronized nodes group together when plotted on a common unit circle, since the transformation (15) affects only the repulsive nodes. Hence, the π-states, in which the variables θ_i separate into two diametrically opposed groups according to the sign of κ_i, can be regarded as an artifact of the parametrization.

To make this clear, we write (14) in terms of the φ_i variables as:

$$\dot{\varphi}_i = \omega_i + \frac{\kappa_i}{N}\sum_{j=1}^{N}\sin(\varphi_j - \varphi_i - \alpha_j), \tag{16}$$

where the phase lag now appears under the sum as α_j, but leaving the dynamics of the system unchanged. The transformation of (1) into (16) by means of (15), with α_i given

by (13), moves the sign of the coupling constant κ_i from outside the sum, as $\operatorname{sgn}\kappa_i$, to inside the sum as $\operatorname{sgn}\kappa_j$. This means that the equations

$$\dot{\theta}_i = \omega_i + \frac{1}{N}\sum_{j=1}^{N} \kappa_j \sin(\theta_j - \theta_i) \tag{17}$$

can be equivalently written as

$$\dot{\varphi}_i = \omega_i + \frac{\operatorname{sgn}\kappa_i}{N}\sum_{j=1}^{N} |\kappa_j| \sin(\varphi_j - \varphi_i), \tag{18}$$

where $\varphi_i = \theta_i - \alpha_i$, i.e. the signs can always be placed outside the sum, for either model (1) or (17).

The two models (1) and (17) have been discussed by Hong and Strogatz [2, 19] with the conclusion that for the latter model "the π-state and travelling-wave state do not appear for the coupling type considered here" and that putting the coupling inside the sum "makes a world of difference". As we have shown, however, the two models are closely related since the signs can appear equivalently outside or inside the sum. Indeed, for the simplest case in which $|\kappa_i| = \kappa$ is independent of the node i, i.e. every coupling is given by $\kappa_i = \pm\kappa$ for some scaling parameter κ, the two models are dynamically identical, being related by the transformation (15). There are significant differences, however, in other cases particularly for very small or large coupling strengths; for example synchronization in the model (1) is sensitive to any small value of $\hat{\kappa}_i$, with a correspondingly large scaling parameter κ being required in order to synchronize the system. (This is because in the limit $\kappa_i \to 0$ for some i, the system cannot synchronize because the frequency of the ith node is fixed at ω_i). By contrast, if the coupling κ_j inside the sum is small for some node j, then that node has little influence on the synchronization properties of the system as a whole. This may be understood by viewing the coupling κ_j as the oscillator amplitude, as we now explain.

5. Amplitude dependence

A fundamental property of the standard Kuramoto model is that the dynamics are independent of the oscillator amplitudes, as is evident from the defining equations (1) which involve the phases θ_i but not the amplitudes of the oscillators. As a consequence each oscillator, even one with a vanishingly small amplitude, contributes equally to the synchronized frequency $\Omega = \sum_i \omega_i/N$ (putting $\kappa_i = \kappa$ in (8)). Amplitude independence was first assumed by Winfree [23] (1967) who argued that in the limit of weak coupling amplitude variations could be neglected, and that the oscillators could be described solely by their phases along their limit cycles. This "phase model reduction" was also used (1975) by Kuramoto [24] and later others [25], but we show that the assumption of uniform amplitudes is unnecessary. In any case, there are models where amplitude variations are significant (such as optomechanical arrays [26]) indeed, the dynamics of large systems which allow time-varying amplitudes have long been studied, see for

example [27] (1991). Amplitude independence is essential, however, when the Kuramoto model is regarded as a quantum system, since such systems are measured by probabilities that are ratios of amplitudes, i.e. physical properties are invariant under a rescaling of local wavefunctions $|\psi_i\rangle$. The Kuramoto model (1) can be viewed as a spin 0 nonlinear quantum system [28], with the normalized wavefunction given by $|\psi_i\rangle = \mathrm{e}^{-\mathrm{i}\theta_i}$, and has amplitude independent properties, as is appropriate for a quantum system.

Distributed amplitudes which are constant in time but vary according to the node, without restriction, can be incorporated into the Kuramoto model by first writing the N defining equations in the following complex form (a special case of the matrix equations given by equation (2) in [29]):

$$\mathrm{i}\dot{z}_i z_i^{-1} = \omega_i - \frac{\mathrm{i}\kappa_i'}{2N}\sum_{j=1}^{N} a_{ij}\left(z_i\, z_j^* - z_j\, z_i^*\right), \tag{19}$$

where z_i is a complex function of t, κ_i' are real parameters and (a_{ij}) is any real matrix. The right hand side of (19) is real and therefore $\mathrm{i}\dot{z}_i z_i^{-1} = -\mathrm{i}(z_i^{-1})^*\dot{z}_i^*$, which implies that $z_i^* z_i$, and hence the amplitude, is constant at each node i. The N complex equations (19) are the Euler-Lagrange equations of a Lagrangian in which the amplitudes are constrained to take constant values by means of Lagrange multipliers. More general oscillator models with distributed amplitudes that are constant in time can also be constructed by choosing the right hand side of (19) to be any real function of the complex variables.

Parametrizing $z_i = \lambda_i \mathrm{e}^{-\mathrm{i}\theta_i}$, we may write (19) as

$$\dot{\theta}_i = \omega_i + \frac{\kappa_i}{N}\sum_{j=1}^{N} a_{ij}\lambda_j \sin(\theta_j - \theta_i), \tag{20}$$

where $\kappa_i = \kappa_i'\lambda_i$. Evidently these equations combine the two models (1,17) proposed in [2, 19], with the coupling parameter λ_j inside the sum now regarded as the constant oscillator amplitude. This requires λ_j to be positive for all j but, as shown in equations (18), negative signs can be moved outside the sum by the change of variable (15). Models in which the summand contains the symmetric combination $\lambda_i\lambda_j$ as in (20) are well-known, see for example Daido [30] (1987) where the corresponding parameters s_i are regarded as random variables. The model (20) has previously been considered also in [31], but only for positive values of the coupling constants.

5.1. Synchronized frequency

We derive an explicit frequency formula, valid for arbitrary amplitudes λ_i, which generalizes the formula (8) for the common frequency Ω of oscillation in the synchronized system. Multiply both sides of (20) by λ_i/κ_i and sum over i to obtain:

$$\sum_{i=1}^{N}\frac{\lambda_i\dot{\theta}_i}{\kappa_i} = \sum_{i=1}^{N}\frac{\lambda_i\omega_i}{\kappa_i} + \frac{1}{N}\sum_{i,j} a_{ij}\lambda_i\lambda_j\sin(\theta_j - \theta_i), \tag{21}$$

where, assuming now that (a_{ij}) is a symmetric matrix, the last term vanishes by symmetry (interchanging i, j). For synchronized solutions we have, from (2), $\Omega = \dot{\theta}_i$ to give:

$$\Omega = \left(\sum_{i=1}^{N} \frac{\lambda_i \omega_i}{\kappa_i} \right) \Big/ \left(\sum_{i=1}^{N} \frac{\lambda_i}{\kappa_i} \right). \tag{22}$$

This formula has properties similar to (8), for example Ω is invariant under separate rescaling of the parameters κ_i, λ_i, and can become arbitrarily large for small values of the denominator and, as before, can always be set to zero by choosing a suitable rotating reference frame. The formula (22) also applies to synchronized systems with nontrivial network topologies, such as those considered in [4, 5, 14]; it is necessary only that (a_{ij}) be symmetric.

Equation (21) can be integrated to obtain a nontrivial constant of the motion:

$$\sum_{i=1}^{N} \frac{\lambda_i \theta_i(t)}{\kappa_i} = t \sum_{i=1}^{N} \frac{\lambda_i \omega_i}{\kappa_i} + \sum_{i=1}^{N} \frac{\lambda_i \theta_i(0)}{\kappa_i}, \tag{23}$$

where $\theta_i(0)$ are the initial values of the system. This equation holds exactly at all times for all solutions of (20), whether the system has synchronized or not. It may be used to eliminate any angle in favour of the remaining angles or, alternatively, as described in Section 3.1, to provide a check on the numerical accuracy of any computation.

5.2. Static equations and critical parameters

We demonstrate that there exist critical values of the parameters κ_i, λ_i which determine the onset of synchronization, by deriving properties of the static equations which the synchronized system must satisfy. In this case $\mathrm{i}\dot{z}_i z_i^{-1} = \Omega$ and so, substituting $z_i = x_i + \mathrm{i}y_i$ into (19), we find that the following $2N$ equations, quadratic in the $2N$ real variables x_i, y_i, must be satisfied:

$$\frac{1}{N} \sum_{j \neq i} a_{ij}(x_j y_i - x_i y_j) = \frac{\Omega - \omega_i}{\kappa_i'}, \quad x_i^2 + y_i^2 = \lambda_i^2. \tag{24}$$

Define

$$a_i = \frac{1}{N} \sum_{j \neq i} a_{ij} y_j, \quad b_i = \frac{1}{N} \sum_{j \neq i} a_{ij} x_j, \quad c_i = \frac{\lambda_i(\Omega - \omega_i)}{\kappa_i}, \tag{25}$$

where $\kappa_i = \kappa_i' \lambda_i$. If we fix the variables x_j, y_j for all $j \neq i$, then a_i, b_i, c_i are also fixed, and (24) describes a straight line $a_i x_i - b_i y_i + c_i = 0$ in the x_i, y_i plane, which must intersect the circle $x_i^2 + y_i^2 = \lambda_i^2$ in order for the system to synchronize. Intersection occurs if and only if

$$|c_i| \leqslant \lambda_i \sqrt{a_i^2 + b_i^2} = \frac{\lambda_i}{N} \Big| \sum_{j \neq i} a_{ij} z_j \Big|, \tag{26}$$

where the synchronized solution z_j takes the form, according to (2), $z_j = \lambda_j \mathrm{e}^{-\mathrm{i}\Omega t} \mathrm{e}^{-\mathrm{i}\theta_j^0}$. There are at most two solutions, corresponding to the plus/minus signs s_i that appear

in (9). Stability considerations determine which of these solutions is attained in the synchronized system.

This geometrical viewpoint shows that critical values of the underlying parameters occur when equality holds in (26) at one or more nodes, i.e. when the line is tangent to the circle in the x_i, y_i plane for some i. If the parameters ω_i, λ_i are fixed then there is a critical value for each κ_i, because for large κ_i the line always intersects the circle (since c_i is small) but as κ_i decreases, a critical point is reached at which the line is tangent to the circle. If we write $\kappa_i = \hat{\kappa}_i\,\kappa$, where κ is defined by (5), and fix $\lambda_i, \omega_i, \hat{\kappa}_i$ while varying κ, then there is also a critical value $\kappa = \kappa_c$ at which the line, for some i, is tangent to the circle. Since c_i decreases as κ increases, solutions to (24) then exist for all $\kappa > \kappa_c$.

It follows from (26) by means of the triangle inequality using $|z_j| = \lambda_j$, or directly from (20), that

$$\left|\frac{\Omega - \omega_i}{\kappa_i}\right| \leqslant \frac{1}{N}\sum_{j\neq i} \lambda_j |a_{ij}|, \tag{27}$$

which comprises a set of N easily-checked inequalities that are necessary, but not sufficient, restrictions on the underlying parameters of the model in order for the system to synchronize. Again, this applies for any symmetric matrix (a_{ij}), and hence for arbitrary network topologies.

5.3. Numerical simulations

We find numerically that synchronized configurations in the model (20), with distributed amplitudes λ_i, appear with properties similar to those found in Sections 3.2–3.4, in particular the grouping of conformist and contrarian nodes corresponds to those shown in figures 1(a,b). If the denominator in the expression (22) is positive, then the conformist/contrarian nodes separate into diametrically opposed groups according to the sign of κ_i, but if the denominator is negative, exactly one repulsive node groups with the conformist nodes similar to that shown in figure 1(b). These configurations are globally stable, like those discussed in Sections 3.2,3.3. There are also locally stable configurations similar to those described in Section 3.4. We provide examples here of all such types for nontrival amplitudes λ_i, including an example of a frustrated configuration for a nontrivial network.

We select the unit N-vector $\hat{\kappa}_i$ with variable signs as described in Section 3.1 and define the couplings $\kappa_i = \kappa\,\hat{\kappa}_i$ for a scaling constant κ of variable magnitude. The positive amplitudes λ_i are selected at random from a uniform distribution in $(0, 1]$ (with an exception for the example shown in figure 3(b) with respect to one negative node), and are normalized so that $\max_i \lambda_i = 1$. We solve the equations in the form (20), with the negative signs placed outside the sum, hence conformist and contrarian nodes do not combine into a single group as observed in [19], but separate into two groups.

For figure 3(a), where $N = 200$ with 120 positive nodes and 80 negative nodes, the denominator in (22) is positive and the synchronized nodes separate into two groups according to the sign of κ_i, with an average phase difference between the two groups

approximately equal to π; this difference, calculated as described in Section 3.2, differs from π by less than 1%. Figure 3(b) shows a synchronized configuration for $N = 200$, with 100 positive and negative couplings each, where for simplicity we have chosen $\hat{\kappa}_i = \pm 1$. The amplitudes are generated randomly as before, except that we have selected one amplitude at a negative node which is two orders of magnitude larger than the remaining amplitudes. This ensures that the denominator in (22) is negative and, similar to the example discussed in Section 3.3, this negative node of largest amplitude groups with the conformist nodes, as shown in figure 3(b). For both examples the systems are globally stable, and we have performed the same numerical checks as described in Section 3.1.

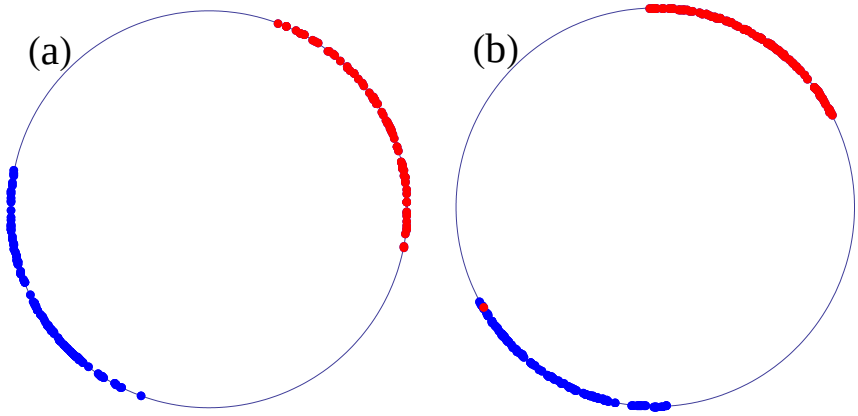

Figure 3. Synchronized configurations with nontrivial amplitudes for $N = 200$ nodes for (a) a positive denominator in equation (22) showing separation into conformist (blue) and contrarian (red) groups, and (b) for a negative denominator showing one repulsive node (in red) grouped with the conformists.

Figures 4(a,b) show two synchronized configurations where frustration is evident, in which one node remains separate from both the conformist and contrarian nodes, even for very large κ. For this example with $N = 40$ there are 24 positive couplings and 16 negative couplings, with the fixed parameters $\hat{\kappa}_i$ and λ_i generated randomly as before. The symmetric connectivity matrix (a_{ij}) is nontrivial, however, with elements equal to either 0 or 1, where the zeroes are generated randomly; in this example 131 of the 780 elements above the diagonal are zero, and the remaining 649 elements are equal to 1. The system always synchronizes, for κ larger than a critical value, to one of the two configurations shown in figures 4(a,b), depending on the initial values. Stability of each configuration is therefore only local. As with the examples in figures 2(a,b), there is also one repulsive node (in red) which groups with the conformist nodes, although here the denominator in (22) is negative, unlike the example of figures 2(a,b). It is noticeable that the relative positions of the nodes in the configurations shown in figures 4(a,b) are maintained even for very large values of κ, as observed also for those in figures 2(a,b).

There are also other locally stable synchronized configurations which appear for various random choices of the underlying parameters $\omega_i, \hat{\kappa}_i, (a_{ij})$, generally for small

N. We briefly mention these in order to show that there are many different possible configurations. In one example an attractive node behaves as a contrarian while another repulsive node is conformist. In another example there are attractive and repulsive nodes neither of which group with the conformist nor the contrarian nodes, i.e. frustrated nodes can be a mixture of both attractive and repulsive nodes and, in another example, two conformist nodes group together with the contrarians. As before, we have performed the same numerical checks as described in Section 3.1, for example the exact solution (23) is satisfied within the preset tolerance at all times, and the synchronization property, that $\sum_i |\dot{\theta}_i - \Omega|$ is zero within tolerance at or near $t = t_{\text{final}}$, is also verified, as are the equations (24) which define the synchronization manifold. The computed frequency Ω agrees with (22) in all cases, confirming that this formula is valid also for nontrivial network topologies.

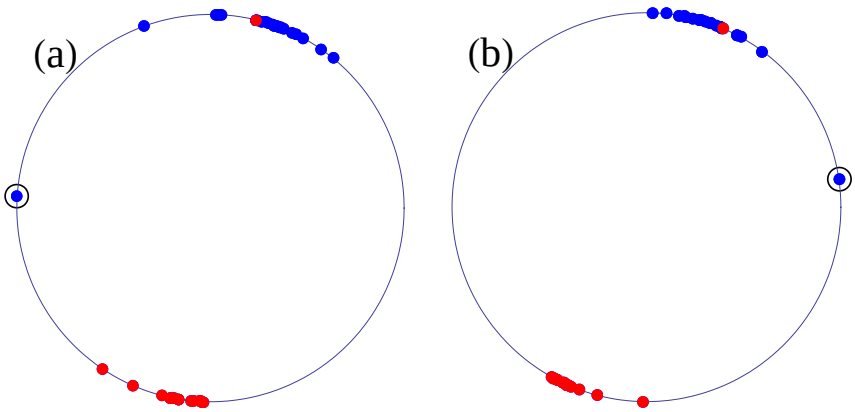

Figure 4. An example for $N = 40$ with nontrivial network couplings, showing two synchronized configurations for identical parameters but different initial values; the frustrated node (circled) is neither conformist nor contrarian, even for large κ.

6. Conclusion

We have investigated the Kuramoto model in which the distributed couplings can have variable sign, and have shown numerically that various stable synchronized configurations can occur, including some with frustrated nodes that are neither conformist nor contrarian. We have found that attractive/repulsive nodes do not always correspond to conformist/contrarian nodes, respectively, in the synchronized system. We have considered the models proposed in [2, 19], with the couplings either outside or inside the sum, and in the combined form (20), and have shown that although the two models are similar or even identical in some cases, there are significant differences at very small couplings κ_i, as is evident from the explicit frequency formulas. We have interpreted the parameters λ_i under the sum as oscillator amplitudes, thereby providing a means of investigating the effects of both small and large amplitude variations on synchronization. We have shown by geometrical arguments that the underlying parameters of the model

must exceed certain critical values and have also derived conditions such as (27), which are necessary for synchronization to occur.

Because of their numerous applications we believe that these models merit further investigation, in particular we have found that repulsive couplings affect synchronization in subtle ways which requires further study. A minimum number of positive couplings, for example, is necessary for synchronization to occur, even at large coupling strengths, depending on the model parameters in ways that are not yet understood.

References

[1] Arenas A, Díaz-Guilera A, Kurths J, Moreno Y and Zhou C 2008 *Phys. Rep.* **469** 93
[2] Hong H and Strogatz S H 2011 *Phys. Rev. Lett.* **106** 054102
[3] Louzada V H P, Araújo N A M, Andrade J S and Herrmann H J 2012 *Scientific Reports* **2** 658
[4] Tsimring L S, Rulkov N F, Larsen M L and Gabbay M 2005 *Phys. Rev. Lett.* **95** 014101
[5] Zhang X, Ruan Z and Liu Z 2013 *Chaos* **23** 033135
[6] Zanette D H 2005 *Europhys. Lett.* **72** 190
[7] Hong H and Strogatz S H 2012 *Phys. Rev.* E **84** 046202
[8] Daido H 1992 *Phys. Rev. Lett.* **68** 1073
[9] Levnajić Z 2011 *Phys. Rev.* E **84** 016231
Levnajić Z 2012 *Scientific Reports* **2** 967
[10] Iatsenko D, Petkoski S, McClintock P V E and Stefanovska A 2013 *Phys. Rev. Lett.* **110** 064101
[11] Petkoski S, Iatsenko D, Basnarkov L and Stefanovska A 2013 *Phys. Rev.* E **87** 032908
[12] Yuan D, Zhang M and Yang J 2014 *Phys. Rev.* E **89** 012910
[13] Ju P, Dai Q, Cheng H and Yang J 2014 *Phys. Rev.* E **90** 012903
[14] Oh E, Lee D-S, Kahng B and Kim D 2007 *Phys. Rev.* E **75** 011104
[15] Varaiya P, Wu F and Chen R L 1985 *Proc. IEEE* **73** 1703
[16] Dörfler F and Bullo F 2012 *SIAM Journal on Control and Optimization* **50** 1616–1642
[17] Anderson D, Tenzer A, Barlev G, Girvan M, Antonsen T M and Ott E 2012 *Chaos* **22** 013102
[18] Hong H 2014 *Phys. Rev.* E **89** 062924
[19] Hong H and Strogatz S H 2012 *Phys. Rev.* E **85** 056210
[20] Mirollo R E and Strogatz S H 2005 *Physica* D **205** 249
[21] Aeyels D and Rogge J A 2004 *Prog. Theor. Phys.* **112** 921
[22] Sakaguchi H and Kuramoto Y 1986 *Prog. Theor. Phys.* **76** 576
[23] Winfree A T 1967 *J. Theor. Biol.* **16** 15
[24] Kuramoto Y 1975 in *International Symposium on Mathematical Problems in Theoretical Physics* H. Araki (Ed.), *Lect. Notes Phys.* **39** 420
[25] Montbrió E and Pazó D 2011 *Phys. Rev.* E **84** 046206
[26] Heinrich G, Ludwig M, Qian J, Kubala B and Marquardt F 2011 *Phys. Rev. Lett.* **107** 043603
[27] Matthews P C, Mirollo R E and Strogatz S H 1991 *Physica* D **52** 293
[28] Lohe M A 2010 *J. Phys. A: Math. Theor.* **43** 465301
[29] Lohe M A 2009 *J. Phys. A: Math. Theor.* **42** 395101
[30] Daido H 1987 *Prog. Theor. Phys.* **77** 622
[31] Paissan G H and Zanette D H 2008 *Physica* D **237** 818